Elastic instability behind brittle fracture in soft solids

D. Riccobelli,[1] P. Ciarletta,[1] G. Vitale,[2] C. Maurini,[3] and L. Truskinovsky[4,*]

[1] *MOX – Dipartimento di Matematica, Politecnico di Milano, 20133 Milano, Italy*
[2] *Laboratoire de Mecanique des Solides, École Polytechnique, 91128 Palaiseau, France.*
[3] *CNRS, Institut Jean Le Rond d'Alembert, Sorbonne Université, UMR 7190, 75005 Paris, France.*
[4] *ESPCI ParisTech, PMMH, CNRS – UMR 7636, 75005 Paris, France.*

We argue that nucleation of brittle cracks in initially flawless soft elastic solids is preceded by a continuum instability which cannot be captured without accounting for geometrically and physical nonlinearities of the constitutive response. To corroborate this somewhat counterintuitive claim, we present a theoretical and numerical study of the simplest model where a homogeneous elastic body subjected to tension is weakened by a free surface which then serves as a site of crack nucleation. We show that in this prototypical setting, brittle fracture starts as a symmetry breaking elastic instability activated by softening and involving large elastic rotations. The implied bifurcation of the homogeneous elastic equilibrium is highly unconventional due to its extraordinary sensitivity to geometry, reminiscent of the transition to turbulence. We trace the development of the instability beyond the limits of continuum elasticity by using quasi-continuum theory allowing one to capture the ultimate strain localization indicative of the formation of actual cracks.

While linearized elasticity theory is usually sufficient in problems involving *propagation* of pre-existing cracks [1–3], we present a compelling evidence that at least for some classes of soft materials the description of crack *nucleation* requires an account of both geometrically and physical elastic nonlinearity [4, 5]. To elucidate the physical origin of the failure of linear theory, we use in this Letter the simplest geometrically exact setting of nonlinear elasticity to study a tensile instability leading to surface fracture.

The phenomenon of surface fracture is of considerable recent interest because the sub-micron parts employed in many modern applications are effectively defect free and their fracture usually originates on unconstrained external surfaces [6]. Crack nucleation at the surface is also of importance for the understanding of the fragmentation of coatings and other brittle surface layers [7–9]. More generally, the emergence of surface fracture patterns [10, 11] is an example of a symmetry breaking instability which is at the heart of complexity development in soft matter physics [12, 13] and biophysics [14, 15].

Nonlinear elastic instabilities were studied extensively in the context of compressive buckling [16–24]. Tensile instability modes, such as necking, wrinkling and shear banding, were studied as well [25–29], however their relation to fracture has been largely overlooked. While several studies have linked bulk crack nucleation with material softening and advanced various phenomenological nucleation criteria [10, 30–37], an understanding on how such criteria relate to the subtle interplay between geometric and physical nonlinearities along the crack nucleation path, remains obscure.

In this Letter we explore both linear and nonlinear stages of the tensile instability which culminates in the formation of cracks. This instability is of spinodal type [38–40] in its peculiar form associated with a surface [41–45]. The degenerate nature of this instability [46] leads to a rather remarkable sensitivity of the emerging patterns to sample geometry. Such behavior, however, is typical for systems with diverging correlation length and is reminiscent of a transition to turbulence.

We show further that the above symmetry breaking elastic instability serves as a precursor of the subsequent ultimate strain localization. The emerging strain singularities render the scale-free continuum elasticity inadequate. To describe the role of micro-scales we resort to a phase-field-type extension of our continuum theory [33, 47–49] which already allows one to model subcontinuum fields representing developed cracks.

Consider a 2D rectangular body $\Omega = [-L,\, L] \times [0,\, H]$. Denote by $\mathbf{x} \in \Omega$ points in the reference configuration and by $\mathbf{y}(\mathbf{x})$ their deformed position, see Fig. 1. Using directly the deformation gradient $\mathsf{F} = \nabla \mathbf{y}$ we account for *geometric* nonlinearities; its singular values $\lambda_{1,2}$ describe stretches in coordinate directions while rotations remain non-linearized [17].

Suppose that the body Ω is loaded in a two-sided hard device, such that $y_1 = \lambda x_1$ at $x_1 = \pm L$, where λ is the applied stretch which serves as the control parameter of the problem. We assume that the material is incompressible, so that $\det \mathsf{F} = \lambda_1 \lambda_2 = 1$, and isotropic, so that the elastic energy density can be written as $\hat{w}(\lambda_1) = w(\lambda_1, \lambda_1^{-1})$. The force balance is then $\nabla \cdot \mathsf{P} = 0$, where P_{ij} are the components of the first Piola-Kirchhoff stress ten-

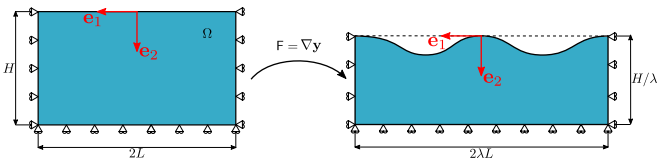

FIG. 1. Schematic representation of the considered surface instability showing the reference and the actual configurations, while also detailing the nature of the boundary conditions.

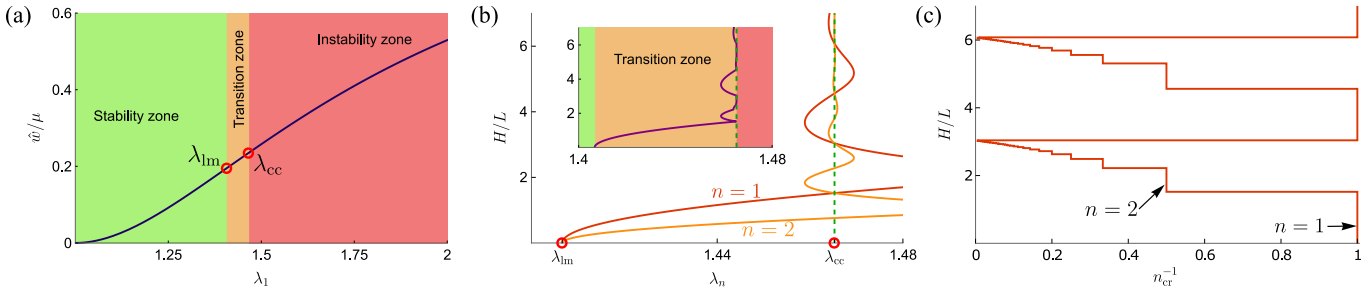

FIG. 2. (a) The energy density $\hat{w}(\lambda)$ of our softening material as a function of the maximal principal stretch λ_1. (b) The stability curves for the two modes with $n = 1$, 2; the purple line in the inset represents the function $\lambda_{\rm cr}(H/L)$. (C) The inverse of the critical mode $n_{\rm cr}$ versus the aspect ratio H/L.

sor $\mathsf{P} = \partial w/\partial \mathsf{F} + p\mathsf{F}^{-1}$ and p is the Lagrange multiplier enforcing the incompressibility constraint. On the side boundaries $x_1 = \pm L$ we impose $y_1 = \pm\lambda L$ together with the free sliding condition $P_{12} = 0$; the upper boundary $x_2 = 0$ is assumed to be free so that $P_{22} = P_{21} = 0$; the lower boundary $x_2 = H$ will be constrained only vertically so that $y_2 = H/\lambda$ and $P_{21} = 0$.

The formulated elastic problem admits a homogeneous solution $\mathbf{y}^{(0)} := \mathsf{F}^{(0)}\mathbf{x}$, where $\mathsf{F}^{(0)} = \mathrm{diag}\,(\lambda, \lambda^{-1})$; the corresponding pressure is $p^{(0)} := -\lambda^{-1}\partial w/\partial\lambda_2$. To study the stability of this solution, we use standard methods [19, 50–52] and write the perturbed displacement and pressure fields, in the form $\mathbf{y} = \mathbf{y}^{(0)} + \sum_{j=1}^{\infty}\varepsilon^j\mathbf{u}^{(j)}$ and $p = p^{(0)} + \sum_{j=1}^{\infty}\varepsilon^j p^{(j)}$ where ε is a small parameter. Inserting these expansions in the force balance we obtain, at the first order, a linear boundary value problem for $\mathbf{u}^{(1)}$ and $p^{(1)}$ which can be solved explicitly. Introducing the stream function $\mathbf{u}^{(1)} = (\partial_2\chi, -\partial_1\chi)$, we obtain $\chi = iAg(\gamma x_2)\exp(i\gamma x_1)/\gamma + \text{c.c.}$, where A is still undefined complex amplitude and c.c. denotes complex conjugate. We have also introduced $\gamma = (n\pi)/(2\lambda L)$ the horizontal wavenumber, where n is an integer with even (odd) values representing symmetric (asymmetric) modes, respectively.

Following closely [19], we write the real valued function g in the form $g(\gamma x_2) = \sum_{k=1}^{4} C_k \exp[\gamma\omega_k\, x_2]$, where $\omega_1 = -\omega_2 = \alpha$, $\omega_3 = -\omega_4 = \beta$. The constants α, β can be found from the relations $\alpha\beta = \lambda^2$ and $\alpha^2 + \beta^2 + 2 = \lambda(\lambda^4 - 1)\eta$; the elastic energy enters these relations through the function $\eta(\lambda) = \hat{w}''(\lambda)/\hat{w}'(\lambda)$ which characterizes the *physical* nonlinearity.

In a body with the aspect ratio H/L, the elastic instability, anticipating the nucleation of cracks, can take place at the bifurcation points $\lambda_n(H/L)$. They are parametrized by the integers $n(H/L)$ which can be found from the condition that there exist a nontrivial set of coefficients C_k, such that the corresponding solution $(\mathbf{u}^{(1)}, p^{(1)})$ satisfies the boundary conditions at the linear order. We can then define $\lambda_{\rm cr}(H/L) = \min_{n\geq 1}\lambda_n(H/L)$ and denote by $n_{\rm cr}(H/L)$ the corresponding critical value of the parameter.

The function $\lambda_{\rm cr}(H/L)$ characterizes the sensitivity of the instability threshold to the geometry of the domain. To illustrate this dependence, we consider a typical energy density with strain softening: $w = \mu\,(I-2)/I$, where $I = \lambda_1^2 + \lambda_2^2$ is the first strain invariant and μ is the measure of rigidity. In this case $\hat{w}(\lambda) = \mu(\lambda^2-1)^2/(2(\lambda^4+1))$ and the softening ($\hat{w}'' < 0$) takes place for $\lambda > \lambda_{\rm lm} = \sqrt[4]{(1/3)\left(\sqrt{33}+6\right)}$, see Fig. 2(a). The value $\lambda_{\rm lm}$ is known as the Considère or the load maximum (LM) threshold [52–54], where by the 'load' we understand the axial stress $P(\lambda) = \mathbf{e}_1\cdot\mathsf{P}\cdot\mathbf{e}_1 = \hat{w}'(\lambda)$ in the direction of traction; reaching this threshold indicates the occurrence of necking in slender bodies [19, 25, 55, 56].

We observe that, independently of the value of n, the functions $\lambda_n(H/L)$, illustrated in Fig. 2(b) for $n = 1, 2$, approach the point $\lambda_{\rm lm} \simeq 1.407$ in the limit infinitely small aspect ratios ($H \ll L$, thin domains, necking, $n_{\rm cr} = 1$) and the point $\lambda_{\rm cc} \simeq 1.465$ in the limit of infinitely large aspect ratios ($H \gg L$, thick domains). The threshold $\lambda_{\rm cc}$ indicates the failure of the complementing condition (CC); in an infinite system such a threshold marks the onset of wrinkling instability where all wave numbers become unstable simultaneously. This leads to ultimate localization of the the unstable modes around a free boundary [43, 45, 57–59]. In our case the value of the CC threshold can be found analytically from the equation $\eta(\lambda_{\rm cc}) = -\lambda_{\rm cc}^{-3}$. In the classical geometrically linearized elasticity theory, where it is assumed that both deformation and rotations are small, and instead of $w(\mathsf{F}^T\mathsf{F})$ we use $w(\mathsf{E})$, where $\mathsf{E} = (1/2)(\nabla\mathbf{u} + \nabla\mathbf{u}^T)$, the very difference between the thresholds $\lambda_{\rm cc}$ and $\lambda_{\rm lm}$ disappears and the whole complexity of the emerging stability diagram (see below) is completely lost.

Outside these two easily accessible limits (of infinitely thin and infinitely thick domains), the function $\lambda_{\rm cr}(H/L)$ shown in the inset in Fig.2(b), looks rather disorderly. However, the underlying rich and complex structure is revealed if we consider instead the integer valued function $n_{\rm cr}(H/L)$, see Fig.2(c). First of all, we observe that the necking-type instability with $n_{\rm cr} = 1$ is not a feature of slender bodies only, but appears periodically as

one changes the aspect ratio. Similarly, the wrinkling-type instability with $n_{\rm cr} = \infty$ appears at periodically distributed values of the aspect ratio; the corresponding period $4\lambda_{\rm cc}^3/\sqrt{-1+2\lambda_{\rm cc}^2+3\lambda_{\rm cc}^4}$ can be computed analytically since in the corresponding points H/L the eigenvalues α and β become complex conjugate and independent of n. Between these special regimes we observe an apparently periodic distribution of 'staircase' structures with infinite number of steps in every period representing all integer values of $n_{\rm cr}$. Each of these 'staircases' demonstrates the same 'devilish' behavior near the accumulation points, which all correspond to recurrent wrinkling thresholds.

The above structure of the stability thresholds can be corroborated by the observation that for $H/L \gg 1$ (when $\lambda_{\rm cr} \sim \lambda_{\rm cc}$) one can approximate the actual problem of finding $n_{\rm cr}(H/L)$, involving minimization of an implicitly given function over a discrete set, by a model problem $\xi_{\rm cr} = \arg\max_\xi(\sin(a\xi)/e^\xi)$, where ξ is a positive integer and $a \sim H/L$. The model problem can be solved explicitly and its solution $\xi_{\rm cr}(a)$ can be formally proved to exhibit the periodic staircase structure of the type shown in Fig.2(c). In physical terms one can argue that in each period the system undergoes a scale-free crossover between necking and wrinkling. The steps of the function $n_{\rm cr}(H/L)$ emerge due to the locking phenomenon in the ranges of aspect ratio H/L where both horizontal and vertical oscillations of the displacement field can remain resonant with the domain geometry. We emphasize the extreme sensitivity of the critical wave numbers to the aspect ratio at special geometries where the instability pattern is changing dramatically from fully localized to fully de-localized. The implied coexistence of vastly different scales is characteristic of spinodals in elastic systems exhibiting long range interactions [38, 60].

To complement the linear stability analysis and to determine the nature of the associated bifurcations, we now perform a standard weakly nonlinear study known as the amplitude expansion in physics [61–64] and as Koiter's postbuckling analysis in mechanics [4, 65–67]. It reduces to finding the next terms of the perturbative expansion $\mathbf{u}^{(2)}$ and $p^{(2)}$ and in particular, allows one to determine the dependence of the amplitude A from the first order expansion on the loading parameter λ.

We start with the 'near necking' regimes where the buckling thresholds λ_n are well separated and only a finite number of modes are initially activated in the postbuckling regime. In this case the natural small parameter is $\varepsilon = \sqrt{|\lambda-\lambda_{\rm cr}|/\lambda_{\rm cr}}$. By expanding the energy functional $\mathcal{W} = \int_\Omega w\,{\rm d}\mathbf{x}$ we obtain $\Delta\mathcal{W} = \varepsilon^4(\theta_2|A|^2 + \theta_4|A|^4) + o(\varepsilon^4)$, where $\theta_2(\lambda)$, $\theta_4(\lambda)$ are known real functions. The requirement of stationarity of the energy in A (at order ε^4), gives the expression for the amplitude $A = \sqrt{-\theta_2/(2\theta_4)}$ which, since in the considered regime θ_2 and θ_4 have the same sign, characterize the bifurcation

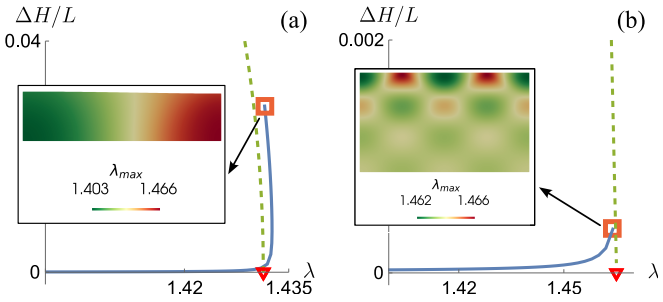

FIG. 3. Bifurcation diagrams showing the amplitude ΔH of the unstable mode on the free surface for the cases: (a) $H/L = 1$ (near necking case) and (b) $H/L = 2.5$ (near wrinkling case). The red triangles denote the critical thresholds $\lambda_{\rm cr}$. Solid and dashed lines represent the results of the finite element simulations and of the weakly non-linear analysis, respectively. Insets show the distribution of the maximal principal stretch $\lambda_{\rm max}$ in the actual configuration corresponding to the location of the square marker.

as a subcritical (unstable) pitchfork, see the dashed line in Fig. 3 (a). The unstable postbuckling is the diffuse necking illustrated in the inset in Fig. 3(a).

The 'near wrinkling' regimes, where buckling thresholds accumulate, are rather different. In this case a small increment of the control parameter λ away from the critical value $\lambda_{\rm cr}$ activates an essentially infinite number of instability modes. Therefore in the weakly nonlinear approximation an unstable mode interacts with many marginally unstable modes. The availability of a broad bandwidth of such modes requires a different scaling and the the natural small parameter in this case is $\varepsilon = |\lambda-\lambda_{\rm cr}|/\lambda_{\rm cr}$, see [68, 69] for similar analyses. In order to take into account all the implied interactions we also need to modify the expression for the stream function $\chi = \sum_{m=-\infty}^{+\infty} i(A_m/\gamma m)g(\gamma m x_2)\exp(i\gamma m x_1) + {\rm c.c.}$ where m is an integer and A_m is amplitude of the mode m. We can then proceed as before and find the amplitude equation, accounting for cubic resonances, in the form of an infinite system $\theta_1 A_m + \sum_{k=-\infty}^{+\infty} \theta_{3(k)} A_k A_{m-k} = 0$. Here the functions $\theta_1(\lambda;m)$ and $\theta_{3(k)}(\lambda;m)$ are again known explicitly. The bifurcation is a subcritical pitchfork, see the dashed line in Fig. 3(b), and the incipient postbifurcational mode, illustrated in the inset in Fig. 3(b) is again unstable.

To complement this semi-analytical analysis we also performed a numerical study of the nonlinear elastic problem in the post bifurcational regime. We assumed that the energy density is of the form $w = (\mu/I)(I - 2\log J - 2) + (\Lambda/2)(\log J)^2$, where $J = \lambda_1\lambda_2$. For numerical convenience the material was taken to be almost incompressible with Λ equal to 100μ; note that as $\Lambda \to +\infty$ we recover both the original energy density and the incompressibility condition.

To recover the bifurcated branch we introduced a

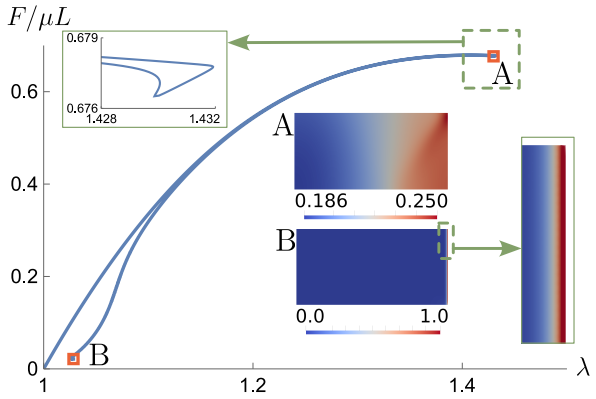

FIG. 4. Normalized axial force $F/\mu L$ versus the mean stretch λ for the near necking case ($H/L = 1$). The insets on the right show the distribution of the phase field variable α in the reference configuration corresponding to the points A and B. The parameter $\ell_0/H = 0.01$.

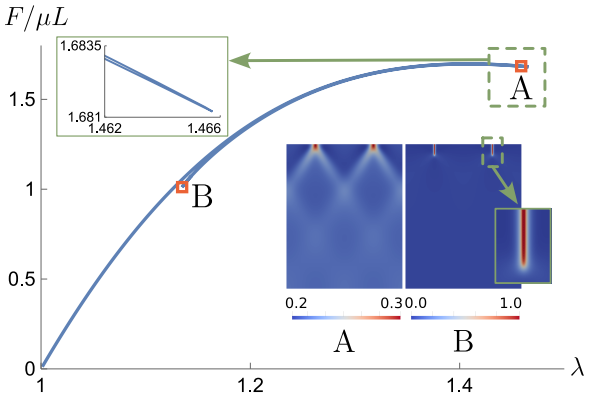

FIG. 5. Normalized axial force $F/\mu L$ versus the mean stretch λ for the near wrinkling case ($H/L = 2.5$). The insets on the right show the distribution of the phase field variable α in the reference configuration corresponding to the points A and B. The parameter $\ell_0/H = 0.01$.

small imperfection on the stress free boundary with a wavenumber of the instability mode and a small amplitude of the order of $10^{-5}\,L$. We then used an arclength continuation method [70, 71] which allowed us to extend the bifurcated branch all the way till an extreme strain focusing caused the local violation of the complementing condition, see the blue lines in Fig. 3(a,b). The obtained deformation patterns at the implied limit of the applicability of continuum elasticity are illustrated in the insets in Fig. 3(a,b) for the typical 'near necking' and 'near wrinkling' regimes.

The ultimate strain localization, which caused the break down of our nonlinear elasticity model, is indicative of the emergence of actual cracks. To capture the latter, the scale-free continuum theory, which is expected to operate only on long waves, can be regularized through the introduction of a sub-continuum length scale. A convenient quasi-continuum approach of this type is a phase-field model of fracture [47, 48]. We can assume, for instance, that $w_{\rm pf} = (1-\alpha)^2(\mu/2)(I-2)+\mu\alpha^2+\mu\,\ell_0^2\|\nabla\alpha\|^2$, where we introduced the damage-like scalar field $\alpha(\mathbf{x}) \in [0,1]$ and complemented the energy density with an additional term penalizing the gradient of α; the compatibility with our original nonlinear elasticity model is ensured by the fact that $w = \min_{\alpha\in[0,1]}[(1-\alpha)^2(\mu/2)(I-2)+\mu\alpha^2]$. The new internal length ℓ_0 serves as a cut-off preventing ultimate strain localization and at $\ell_0 \ll L$, we obtain a Griffith-like fracture model with the finite toughness $G_c = \mu\ell_0/2$ [33, 47, 72].

Using the phase field type model and adopting again the weak compressibility regularization, we reproduced and considerably extended the post-bifurcational results obtained above. To minimize at each value of the loading parameter λ the energy with respect to both, the deformation field $\mathbf{y}(\mathbf{x})$ and the phase-field $\alpha(\mathbf{x})$, we used a Newton's algorithm complemented by a standard pseudo-arclength continuation technique [70]. The results of the two representative numerical simulations, illustrating qualitatively different regimes, are presented in Figs. 4-5: the 'near necking' case with $H/L = 1$ and $\lambda_{\rm cr}$ far from $\lambda_{\rm cc}$ in Fig. 4 and the 'near wrinkling' case with $H/L = 2.5$ and $\lambda_{\rm cr}$ close to $\lambda_{\rm cc}$ in Fig. 5. In both figures the (unstable) post-bifurcational response is illustrated through the dimensionless force-stretch relation $F(\lambda) = \int_{-H}^{0} P_{11}(\lambda)|_{x_1=L}\,{\rm d}x_2$. The deformed fields close and far from the bifurcation points are illustrated in the insets through the phase field distributions which make the emergence of developed cracks more visible. While in our 'near wrinkling' regime we show the formation of two cracks only, it is clear that the aspect ratio of the domain could be chosen to exhibit an arbitrary large number of emerging cracks.

One can see that in both cases shown in Figs. 4-5 the development of elastic instability leads to gradual localization of diffuse damage which precedes the actual formation of cracks. The latter process takes the form of an ultimate localization with the damage parameter reaching the value $\alpha \sim 1$ in the crack-like regions, whose thickness is of order ℓ_0. Since our study is focused on crack nucleation, we did not advance our simulations all the way till the eventual complete break down of the slab. The study of such process would be of interest by itself due to the possibility of secondary bifurcations representing, for instance, crack branching or selective crack arrest [10].

To conclude, using the simplest geometrical setting and focusing on initially flawless soft solids, we showed that crack nucleation is preceded by an elastic instability which can be singled out using conventional engineering elasticity only if the latter is understood as a continuum theory accounting for both geometrical and physical nonlinearities. Such a theory predicts a complex stabil-

ity diagram with geometry-sensitive crossovers between necking and wrinkling modes. Both necking and wrinkling instabilities were shown to result in the formation of developed cracks if the classical elasticity is seamlessly extended as a phase-field type quasi-continuum model. Our analysis builds a bridge between nonlinear elasticity and fracture mechanics and points to the existence of purely elastic precursors of crack nucleation. Similar mechanisms should be operative in other singular manifestations of elasticity such as, for instance, cavitation [73], phase nucleation [74] and creasing [75].

* lev.truskinovsky@espci.fr

[1] L. D. Landau, E. M. Lifshitz, A. M. Kosevich, and L. P. Pitaevskii, *Theory of elasticity: volume 7*, Vol. 7 (Elsevier, 1986).
[2] D. Broek, *The practical use of fracture mechanics* (Springer Science & Business Media, 2012).
[3] K. B. Broberg, *Cracks and fracture* (Elsevier, 1999).
[4] S. S. Antman, *Nonlinear Problems of Elasticity* (Springer, 2005) pp. 513–584.
[5] J. M. Marsden and T. J. R. Hughes, *Mathematical Foundations of Elasticity* (Prentice-Hall Inc., 1983).
[6] G. Dehm, B. N. Jaya, R. Raghavan, and C. Kirchlechner, Acta Mater. **142**, 248 (2018).
[7] J. W. Hutchinson and Z. Suo, Adv. Appl. Mech. **29**, 63 (1991).
[8] H. Colina, L. de Arcangelis, and S. Roux, Phys. Rev. B **48**, 3666 (1993).
[9] U. Handge, Y. Leterrier, G. Rochat, I. Sokolov, and A. Blumen, Phys. Rev. E **62**, 7807 (2000).
[10] B. Bourdin, J.-J. Marigo, C. Maurini, and P. Sicsic, Phys. Rev. Lett. **112**, 014301 (2014).
[11] L. Truskinovsky, G. Vitale, and T. Smit, Int. J. Eng. Sci. **83**, 124 (2014).
[12] J. Kim, J. Yoon, and R. C. Hayward, Mat. Mater. **9**, 159 (2010).
[13] E. Hohlfeld and L. Mahadevan, Phys. Rev. Lett. **106**, 10.1103/PhysRevLett.106.105702 (2011).
[14] M. B. Amar and A. Goriely, J. Mech. Phys. Solids **53**, 2284 (2005).
[15] P. Ciarletta, V. Balbi, and E. Kuhl, Phys. Rev. Lett. **113**, 248101 (2014).
[16] M. A. Biot, *Mechanics of Incremental Deformations* (John Wiley & Sons, 1965).
[17] R. W. Ogden, *Non-Linear Elastic Deformations* (Dover, 1984).
[18] D. Bigoni, *Nonlinear Solid Mechanics: Bifurcation Theory and Material Instability* (Cambridge University Press, 2012).
[19] R. Hill and J. Hutchinson, J. Mech. Phys. Solids **23**, 239 (1975).
[20] G. DelPiero and R. Rizzoni, J. Elast. **93**, 203 (2008).
[21] J. Sivalogathan and S. Spector, Proc. R. Soc. **466**, 1167 (2012).
[22] Y. Grabovsky and L. Truskinovsky, Contin. Mech. Thermodyn. **19**, 211 (2007).
[23] K. Sawyers and R. Rivlin, J. Elast. **12**, 101 (1982).
[24] N. Triantafyllidis, W. M. Scherzinger, and H.-J. Huang, Int. J. Solids Struct. **44**, 3700 (2007).
[25] B. Audoly and J. W. Hutchinson, J. Mech. Phys. Solids **97**, 68 (2016).
[26] Q. Li and T. J. Healey, J. Mech. Phys. Solids **97**, 260 (2016).
[27] E. Cerda and L. Mahadevan, Phys. Rev. Lett. **90**, 074302 (2003).
[28] J. W. Hutchinson and V. Tvergaard, Int. J. Solids Struct. **17**, 451 (1981).
[29] R. Hill and J. Hutchinson, J. Mech. Phys. Solids **23**, 239 (1975).
[30] P. Klein and H. Gao, Eng. Fract. Mech. **61**, 21 (1998).
[31] S. A. Silling, O. Weckner, E. Askari, and F. Bobaru, Int. J. Fract. **162**, 219 (2010).
[32] A. Shekhawat, S. Zapperi, and J. P. Sethna, Phys. Rev. Lett. **110**, 185505 (2013).
[33] E. Tanné, T. Li, B. Bourdin, J.-J. Marigo, and C. Maurini, J. Mech. Phys. Solids **110**, 80 (2018).
[34] A. Kumar, B. Bourdin, G. A. Francfort, and O. Lopez-Pamies, J. Mech. Phys. Solids **142**, 104027 (2020).
[35] P. K. Kristensen, C. F. Niordson, and E. Martínez-Pañeda, Phil. Trans. R. Soc. A **379**, 20210021 (2021).
[36] T. Hao and Z. M. Hossain, Phys. Rev. B **100**, 014204 (2019).
[37] C. J. Larsen, Mech. Res. Commun. **128**, 104059 (2023).
[38] C. J. Gagne, H. Gould, W. Klein, T. Lookman, and A. Saxena, Phys. Rev. Lett. **95**, 095701 (2005).
[39] A. O. Schweiger, K. Barros, and W. Klein, Phys. Rev. E **75**, 031102 (2007).
[40] W. Klein, T. Lookman, A. Saxena, and D. M. Hatch, Phys. Rev. Lett. **88**, 085701 (2002).
[41] H. C. Simpson and S. J. Spector, J. Elast. **15**, 229 (1985).
[42] A. Benallal, R. Billardon, and G. Geymonat, in *Bifurcation and Stability of Dissipative Systems* (Springer, 1993) pp. 1–44.
[43] H. C. Simpson, J. Elast. **139**, 1 (2020).
[44] A. Mielke and P. Sprenger, J. Elast. **51**, 23 (1998).
[45] P. V. Negrón-Marrero and E. Montes-Pizarro, J. Elast. **107**, 151 (2012).
[46] S. G. Mikhlin, Russ. Math. Surv. **28**, 45 (1973).
[47] B. Bourdin, G. Francfort, and J.-J. Marigo, J. Mech. Phys Solids **48**, 797 (2000).
[48] A. Karma, D. A. Kessler, and H. Levine, Phys. Rev. Lett. **87**, 045501 (2001).
[49] O. U. Salman and L. Truskinovsky, J. Mech. Phys. Solids **154**, 104517 (2021).
[50] Y. Cao and J. W. Hutchinson, Proc. R. Soc. A **468**, 94 (2012).
[51] M. A. Holland, B. Li, X. Q. Feng, and E. Kuhl, J. Mech. Phys. Solids **98**, 350 (2017).
[52] J. Li, H. Varner, and T. Cohen, J. Mech. Phys. Solids **172**, 105171 (2023).
[53] I. S. Yasnikov, A. Vinogradov, and Y. Estrin, Scr. Mater. **76**, 37 (2014).
[54] S. M. Fielding, Phys. Rev. Lett. **107**, 258301 (2011).
[55] V. Tvergaard, Comput. Methods Appl. Mech. Eng. **103**, 273 (1993).
[56] A. Needleman, Mech. Mater. **116**, 180 (2018).
[57] M. Šilhavý, *The Mechanics and Thermodynamics of Continuous Media* (Springer Berlin Heidelberg, 1997).
[58] X. Liu and B.-W. Schulze, *Boundary Value Problems with Global Projection Conditions*, Vol. 265 (Springer, 2018).
[59] M. A. Biot, Appl. Sci. Res. **12**, 168 (1963).
[60] H. B. da Rocha and L. Truskinovsky, Phys. Rev. Lett.

124, 015501 (2020).
[61] P. Becherer, A. N. Morozov, and W. van Saarloos, Physica D **238**, 1827 (2009).
[62] M. Weinstein, Proc. R. Soc. A **375**, 155 (1981).
[63] B. Audoly, Phys. Rev. E **84**, 011605 (2011).
[64] Y. Pomeau, S. Zaleski, and P. Manneville, Phys. Rev. A **27**, 2710 (1983).
[65] W. T. Koiter, *On the stability of elastic equilibrium* (National Aeronautics and Space Administration, 1967).
[66] B. Budiansky, Adv. Appl. Mech. **14**, 1 (1974).
[67] A. M. A. van der Heijden, ed., *W. T. Koiter's Elastic Stability of Solids and Structures* (Cambridge University Press, 2008).
[68] Y. B. Fu and R. W. Ogden, Contin. Mech. Thermodyn. **11**, 141 (1999).
[69] P. Ciarletta and Y. Fu, Int. J. Non-Linear Mech. **75**, 38 (2015).
[70] R. Seydel, *Practical bifurcation and stability analysis*, Vol. 5 (Springer Science & Business Media, 2009).
[71] Y. Su, D. Riccobelli, Y. Chen, W. Chen, and P. Ciarletta, Proc. R. Soc. A **479**, 20230358 (2023).
[72] A. A. Griffith, Phil. Trans. R. Soc. Lond. **221**, 163 (1921).
[73] A. Kumar and O. Lopez-Pamies, J. Mech. Phys. Solids **150**, 104359 (2021).
[74] Y. Grabovsky and L. Truskinovsky, J. Nonlinear Sci. **23**, 891 (2013).
[75] P. Ciarletta and L. Truskinovsky, Phys. Rev. Lett. **122**, 248001 (2019).